Polarimetric Rainfall Estimation in the Presence of Anomalous Propagation

ALEXANDER V. RYZHKOV AND DUSAN S. ZRNIC

NOAA, National Severe Storms Laboratory, Norman, Oklahoma

(Manuscript received 3 April 1997, in final form 2 January 1998)

ABSTRACT

Rainfall estimation from specific differential phases in meteorological situations with significant anomalous propagation (AP) is discussed. It is shown that the correlation coefficient between horizontally and vertically polarized backscatter signals and local variability of the total differential phase can be good identifiers of ground clutter–contaminated data. Further, it is suggested how to estimate rainfall in regions of ground clutter caused by AP.

1. Introduction

Anomalous propagation (AP) effects pose a serious problem for accurate radar rainfall measurement. Anomalous propagation conditions exist if the refractive index N in the surface atmospheric layer decreases with height with a rate exceeding $|dN/dh| > 157$ km^{-1} (Bean and Dutton 1966). The radar beam is then trapped within a surface waveguide, producing ground returns at great distances from the radar. Meteorological conditions leading to AP echoes typically occur when a temperature inversion in the atmospheric surface layer is concurrent with a sharp vertical decrease of specific humidity. Anomalous propagation conditions in the Great Plains are frequently associated with thunderstorm outflows (''after storm'' superrefraction) or nocturnal radiative cooling (Bean and Dutton 1966; Weber et al. 1993). In contrast with a ground clutter in the near vicinity of the radar, which is rather stable in time and space, AP-induced ground clutter echo is an unpredictable and ephemeral phenomenon.

Because ground clutter's Doppler spectrum is narrow and centered on zero Doppler frequency, the most effective way to mitigate AP contamination is to apply a high-pass filter in the frequency domain. This procedure is used in the WSR-88D radars (Pratte et al. 1995). The high-pass ground clutter filter in all range–azimuth resolution cells eliminates stationary echoes caused by AP. Such filtering has a drawback, however, because the removal of power near zero radial velocity can bias Doppler spectral moment estimates of the weather signal.

There are two aspects of the AP problem: 1) recognition of the regions containing AP-induced ground clutter echoes and 2) rainfall estimation in the regions contaminated with AP ground clutter. The first aspect of the problem can be addressed using some alternative approaches not involving Doppler filtering. One of these is a statistical pattern classification method based on the analysis of reflectivity field structure (Moszkowicz et al. 1994). This method was used to discriminate between ground clutter and weather radar returns with a conventional noncoherent radar. Another approach requires a polarimetric radar. Some researchers (e.g., Ryzhkov et al. 1994) used the cross-correlation coefficient ρ_{hv} between horizontally and vertically polarized returns obtained from noncoherent dual-polarization radar to distinguish ground clutter from precipitation echoes. For weather echoes, the cross-correlation coefficient is usually larger than 0.8, whereas it is considerably lower in areas contaminated with ground clutter. Zrnic and Ryzhkov (1996) indicate that another polarimetric radar variable, differential phase, exhibits very different behavior for weather and ground clutter echoes. The differential phase of ground scatterers is uniformly distributed in the $-180°$–$180°$ interval, whereas it has relatively narrow distribution about its mean for the echoes from clouds and precipitation. The width of this distribution is determined by the magnitude of the cross-correlation coefficient.

This paper explores how polarimetry can cope with the AP problem. Four Oklahoma storms with AP were observed with the National Severe Storms Laboratory's (NSSL) polarimetric radar [10-cm wavelength (Zahrai and Zrnic 1993)]. Here we address mostly the second aspect of the problem of AP, namely, unbiased estimation of rainfall if AP-induced ground clutter is superimposed on the echoes from precipitation.

Corresponding author address: Dr. Alexander V. Ryzhkov, NOAA/NSSL, 1313 Halley Circle, Norman, OK 73069.
E-mail: alexander.ryzhkov@nssl.noaa.gov

© 1998 American Meteorological Society

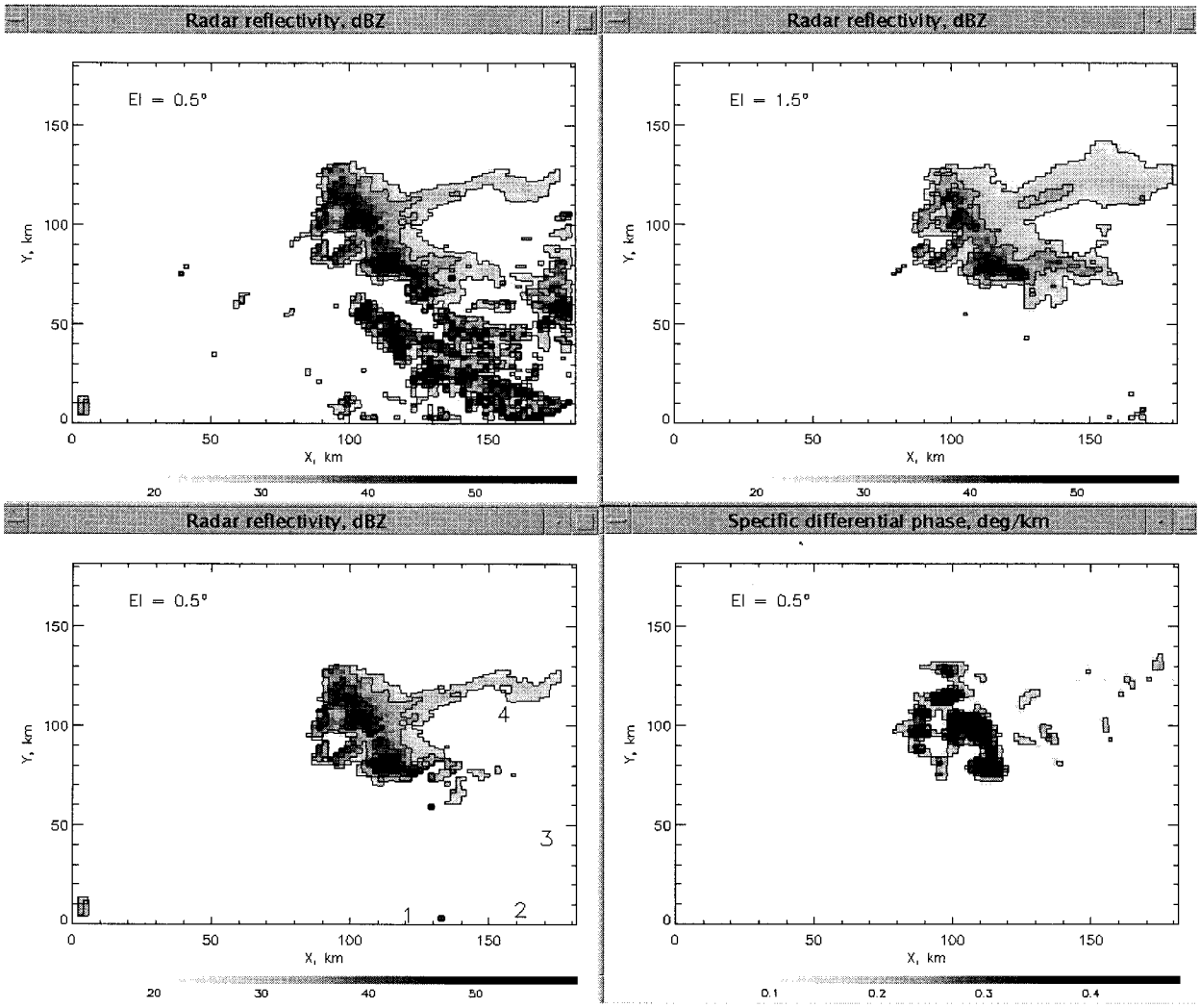

FIG. 1. (a)–(c) Composite plot of radar reflectivity factor Z and (d) specific differential phase K_{DP} for the storm of 7 October 1996: (a) El = 0.5°, (b) El = 1.5°, and (c) El = 0.5°; data with $\rho_{hv} > 0.7$ are plotted. The radar is located at the lower right corner of the images. Contours of Z are 10 dB apart, starting from 20 dBZ. Numbers in (c) indicate the Oklahoma Mesonet gauge locations. The time is 1357 UTC.

2. Polarimetric recognition of AP

The storm of 7 October 1996 had strong and widespread AP echoes caused by nocturnal radiative cooling. Radar observations started in the morning at 1348 UTC (0848 LT). After 1 h of observations the AP echoes almost disappeared. Figure 1a illustrates the radar reflectivity field in the northwestern sector of the radar coverage area at the beginning of observation at 1357 UTC. Rawinsonde data (not shown) taken at 1200 UTC show a well-pronounced temperature inversion in the surface layer with a more than 5°C increase with height within the first 400 m of altitude. The radar reflectivity pattern at the elevation of 0.5° exhibits two ridges that at first glance are almost indistinguishable in terms of the reflectivity structure. More detailed analysis, however, shows that the lower ridge has larger maximal reflectivity (65 dBZ) compared with the upper ridge (54 dBZ). Unusually high reflectivity of the lower ridge suggests that it was produced by the AP effects. This is also implied by the large pixel-to-pixel variations of the reflectivity. Nevertheless, a more definitive conclusion can be made only after the ρ_{hv} field is considered. Our measurements indicate that ρ_{hv} of ground clutter echo is usually in the range between 0.4 and 0.7. Cross correlation for radar returns from precipitation is considerably higher—mostly well above 0.8 (with possible exception of hail or melting-layer regions) with a mean value within the interval 0.9–0.95. Therefore, the ρ_{hv} threshold of 0.7–0.8 can be applied to distinguish between ground clutter and precipitation echoes, unless large hail or the transition region between rain and snow is encountered. The measured cross-correlation coeffi-

cients can be slightly different for different radars observing the same precipitation because ρ_{hv} is affected by the system's performance (similar to Doppler spectrum width) and polarimetric purity (i.e., degree of matching between the antenna patterns at H and V polarizations and cross coupling between orthogonally polarized signals in the antenna and the microwave assembly system). The better the radar system design is, the higher the cross-correlation coefficient is for the same class of hydrometeors. Therefore, the recommended ρ_{hv} threshold for AP discrimination might be radar dependent.

In Fig. 1c the reflectivities for which corresponding values of ρ_{hv} are less than 0.7 have been eliminated. The remaining reflectivity area is attributed to precipitation. This distinction is supported by the information provided by Mesonet rain gauges located in the examined region (see Fig. 1c). Gauges 1–3 located in the AP ground clutter area did not register any rain accumulation during the observation period, whereas gauge 4 situated on the periphery of the supposed precipitation zone indicates a small amount of rain (accumulation of 0.5 mm in 1 h). Another supporting evidence is that the reflectivity region at the higher elevation angle of 1.5° (Fig. 1b), where there is no contribution from ground clutter, is consistent with the image in Fig. 1c. All of these indicators suggest that discrimination between precipitation echo and AP ground clutter echo based on the analysis of the cross-correlation coefficient is quite reliable.

The estimated specific differential phase K_{DP} is shown in Fig. 1d. It is obvious that the current algorithm for estimating K_{DP} automatically eliminates areas contaminated with ground clutter. To explain this performance, some important details of the K_{DP} algorithm are described next. Radials of the total differential phase Φ_{DP} data are used as an input to the algorithm. After dealiasing the Φ_{DP} data (the unambiguous angle is 180°), estimation of the standard deviation (SD) of Φ_{DP} at each range location is made. Normally 17 consecutive range gates are used to compute the SD(Φ_{DP}), which is then assigned to the center of a selected radial interval. If the SD(Φ_{DP}) exceeds the threshold of 12°, the data are classified as noise or ground clutter. Otherwise, it is assigned to the weather signal category and it is smoothed. The gaps between ''signal'' intervals, where noise or ground clutter are present, are bridged by linear interpolation of the smoothed Φ_{DP} data. Thus, if the gap was due to noise or ground clutter with no superposed precipitation, then the smoothed Φ_{DP} would have zero slope and the corresponding specific differential phase K_{DP} would be identically zero. This is exactly the case in Fig. 1d in the AP ground clutter region. If, however, some precipitation were mixed with ground clutter in the gap [and SD(Φ_{DP}) is greater than 12°], the interpolated Φ_{DP} curve would have a nonzero slope due to the contribution from precipitation to the accumulated differential phase. This situation is addressed in more detail at the end of this section and in section 3.

The standard deviation of Φ_{DP} is crucially dependent on the magnitude of the cross-correlation coefficient. The dependence of SD(Φ_{DP}) on ρ_{hv} is specified by the following relation:

$$\mathrm{SD}(\phi_{DP}) = C(|\rho_{hv}|^{-2} - 1)^{1/2}, \qquad (1)$$

where the coefficient C depends on dwell time and Doppler spectrum width (see details of derivation in the appendix). For the NSSL's Cimarron polarimetric radar, the experimentally measured average SD(Φ_{DP}) is about 3°–4°, if ρ_{hv} is about 0.95 (Ryzhkov and Zrnic 1996). According to (1), the corresponding SD(Φ_{DP}) for ρ_{hv} = 0.7 is more than three times higher. Therefore, data with $\rho_{hv} < 0.7$ have a standard error of Φ_{DP} larger than 12°. Hence, if the threshold of $\rho_{hv} = 0.7$ is chosen, discrimination procedures based on the cross-correlation coefficient and the differential phase are well matched. Note, however, that these discrimination procedures are not completely equivalent because the coefficient C in (1) depends on Doppler spectrum width. To just recognize AP, the ρ_{hv}-based method is a viable option because it is very simple and can be easily implemented even on non-Doppler dual-polarization radars (Ryzhkov et al. 1994). If quantitative measurements of precipitation are required in regions of AP mixed with rain, then the K_{DP}-based method is preferred because K_{DP} itself can be used for rainfall estimation.

Maximum estimated K_{DP} in the precipitation area is 1.5° km^{-1}. Rain rates R obtained from Z using the Marshall–Palmer relation or the algorithm on the WSR-88D are somewhat higher than the ones computed from K_{DP} with the formula $R = 40.6K_{DP}^{0.866}$ (Sachidananda and Zrnic 1987). This indicates that a contribution from AP-induced ground clutter might exist in the precipitation area and add to the observed values of the radar reflectivity factor. As will be shown shortly, the polarimetric rainfall estimates often can circumvent this contamination. The actual rainfall recorded by only one gauge (number 4) in the examined area is not enough to validate either the conventional or the polarimetric rainfall estimate. Furthermore, incorrect calibration or choice of the $R(Z)$ relation can also cause discrepancy between the conventional and the polarimetric rainfall estimates.

Note that in the areas characterized by large hail, or in bright band, the cross-correlation coefficient can drop below the threshold of 0.7 and, consequently, SD(Φ_{DP}) can be quite high. To distinguish these two situations from those characterized by AP contamination, examination of differential reflectivity Z_{DR} is required. In the areas of AP echoes, Z_{DR} is very noisy. In contrast, both large hail and bright band exhibit very ''coherent'' Z_{DR} patterns: Z_{DR} is close to zero, or even slightly negative in large hail, whereas the bright band is characterized by large positive values of Z_{DR}.

In the case of 7 October 1996, radar echoes from

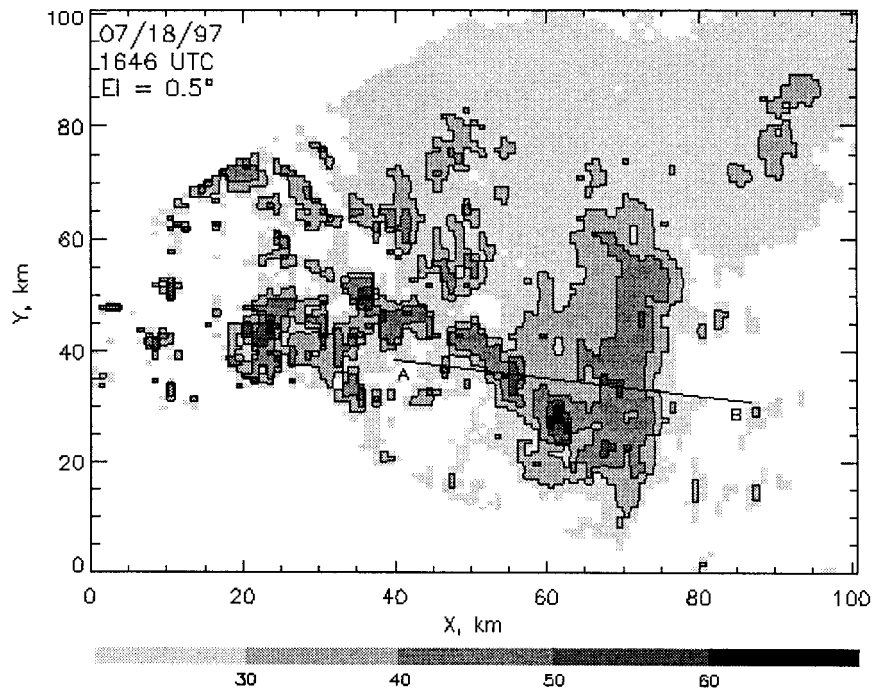

FIG. 2. Field of the radar reflectivity factor for the storm of 18 July 1997. Contours of Z are 10 dB apart, starting at 30 dBZ.

precipitation and AP are clearly separated. This circumstance as well as the obvious difference in the texture of radar reflectivity echo between two ridges makes rain–AP discrimination relatively simple. Such discrimination is more complicated if the echoes from precipitation and AP are overlapped. The storm of 18 July 1997 is a typical example of a situation in which AP echoes are embedded in the precipitation shaft (Fig. 2). In Fig. 2, the radar is located approximately 20 km to the left of the image frame, and the storm is moving to the east, away from the radar. The AP echoes caused by thunderstorm outflow develop just behind the storm at $X < 55$ km and merge with the precipitation echo at $X > 55$ km. It is very difficult to recognize zones of AP contamination in the area of convective precipitation ($55 < X < 75$ km; $15 < Y < 60$ km) using the radar reflectivity and its texture. Only careful analysis of all polarimetric variables available, Φ_{DP}, K_{DP}, Z_{DR}, and ρ_{hv}, together with the radar reflectivity factor Z, allows us to conclude that the AP heavily contaminates rain area to the south of the line AB in Fig. 2, whereas rain echo dominates to the north of this line at $X > 55$ km. Below the line, ρ_{hv} is very low, Φ_{DP} and Z_{DR} are noiselike, and radar reflectivity exceeds 60 dBZ at some points. At the line AB (coinciding with the one of the radar radials), the contributions from AP and rain are comparable (Fig. 3). The polarimetric variable Φ_{DP} is clear from the AP contamination at the elevation of 1.5° and exhibits a steady, slow increase within the range interval between 55 and 75 km (the thick solid line in Fig. 3). At the lower elevation of 0.5°, the AP contamination induces bursts of Φ_{DP} fluctuations at certain range intervals. For the range gates that are free of ground clutter contamination, the Φ_{DP} curves from the two elevations almost coincide (69–76 km, for example). Note that after bridging the gaps between ''good'' range intervals, as prescribed by the algorithm for K_{DP} estimation, the resulting Φ_{DP} curve has a nonzero slope in some regions in which the AP contribution is strong. The slope of Φ_{DP} between 63 and 69 km corresponds to the rain rate of about 10–

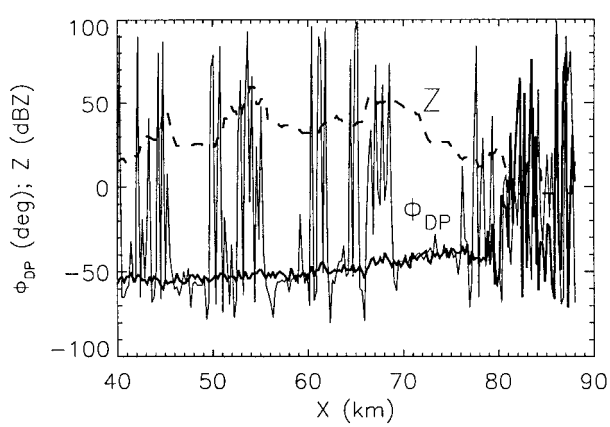

FIG. 3. Radial dependencies of differential phase Φ_{DP} and reflectivity factor Z along the line AB in Fig. 2. The thin solid line represents Φ_{DP} at the elevation of 0.5°, the thick solid line represents Φ_{DP} at the elevation of 1.5°, and the dashed line represents Z at the elevation of 0.5°.

20 mm h^{-1}. Clearly, in this case, the polarimetric technique can quantify rainfall in a region in which strong AP and a rain shaft coincide.

3. Rainfall estimation in the presence of anomalous propagation

For the case of 30 June 1994, we had an opportunity to make a more sophisticated comparison of the estimated rainfall in the presence of AP with the actual rainfall because the AP-contaminated region of precipitation overlapped with the test area containing 42 densely spaced rain gauges in the Little Washita River Basin. This storm's outflow acted as a good duct to cause anomalous propagation (see Fig. 4). The storm was moving from northwest to southeast. Very strong ground clutter echoes due to AP are seen just behind the storm in the precipitation-free area (Y = 125 to 225 km and X = 0 to 130 km). There are some patches of AP-induced ground clutter evident in the precipitation area also, predominantly in the stratiform part of the storm. These zones appear as white holes in the storm's image in Fig. 4b, in which only reflectivities with corresponding $\rho_{hv} > 0.7$ are presented. Some of these white holes fall into the test region outlined by the rectangle.

A composite image of four polarimetric radar variables in the test area is presented in Fig. 5. The time is 0549 UTC, and the elevation angle is 0.5°. Ground clutter contamination is evident in the region of light precipitation in the upper part of the reflectivity field. Very high values of radar reflectivity factor, an intermittent reflectivity pattern, and very low corresponding values of the cross-correlation coefficient locate the anomalous ground clutter. Note that the estimated specific differential phase is relatively unaffected by the AP and suggests very light precipitation in the contaminated area. The performance of the algorithm for K_{DP} estimation is illustrated in Fig. 6, in which the Φ_{DP}, Z, and ρ_{hv} data are presented along a radial through the area with the AP ground clutter. In the intervals in which contribution from ground clutter dominates, Φ_{DP} has large variations with range. These coincide with increases in radar reflectivity factor and significant decreases of the cross-correlation coefficient. As explained in the previous section, after editing and smoothing the Φ_{DP} data, the resulting Φ_{DP} curve has a small nonzero slope in the AP regions—for example, between 65 and 80 km from the radar similar to the case of 18 July 1997. The corresponding K_{DP} is about 0.12° km^{-1} in this range interval, and the rain rate is approximately 6–7 mm h^{-1}.

Anomalous propagation existed for about 1 h in the test area, from 0530 until 0630 UTC. To make radar and gauge data compatible, we have interpolated 1 h of rain accumulations derived from the 42 gauges to the whole basin area (Fig. 7a). The standard Marshall–Palmer formula $Z = 200R^{1.6}$ was used to compute rain rates from the reflectivity factor; these were summed to produce 1-h rain accumulations over the basin area (Fig. 7b). A polarimetric estimate of the areal rain depth was made using specific differential phase. Two different radial averaging intervals were used for estimating K_{DP}: one was over 32 and the other was over 48 adjacent range locations spaced by 0.18 km (Figs. 7c and 7d, respectively).

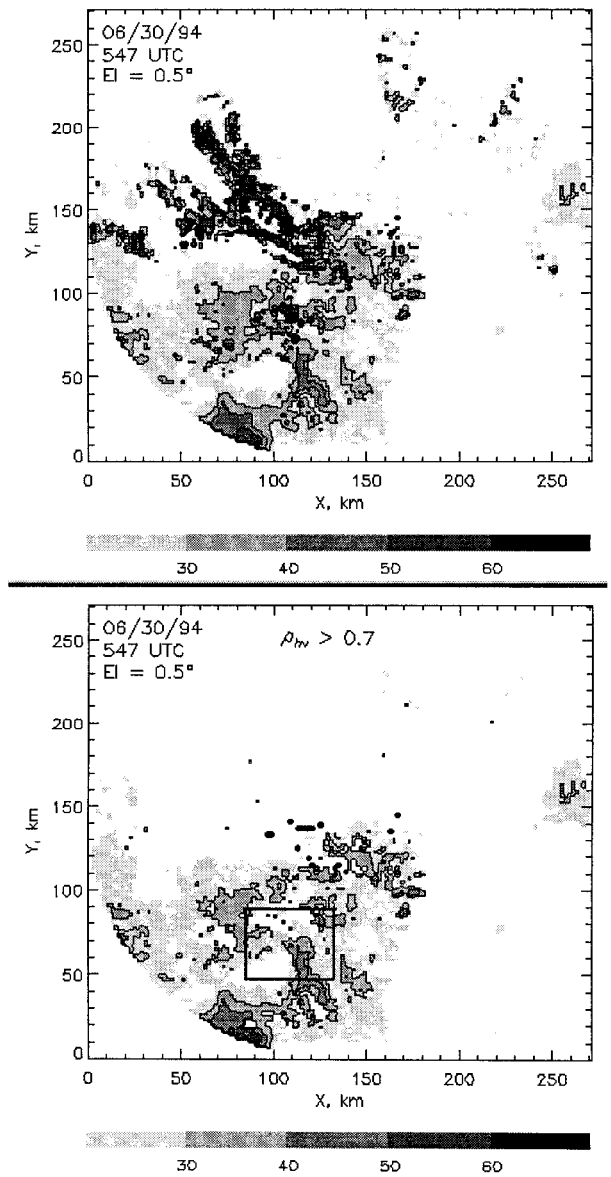

FIG. 4. The plan position indicator of Z at the elevation of 0.5° for the storm of 30 June 1994: (a) all Z are displayed and (b) Z with $\rho_{hv} > 0.7$ are displayed. The white rectangle represents the gauge test area. Contours are drawn every 10 dB, starting at 30 dBZ. The radar is located in the center of the figure.

It is evident that rain accumulations calculated from Z are contaminated by AP clutter at about 90 pixels (size 1 km × 1 km) corresponding to the area of 90 km^2. In some pixels with light rain, false accumulations up to 150 mm were computed. Both polarimetric estimates are immune to AP contamination. We estimate

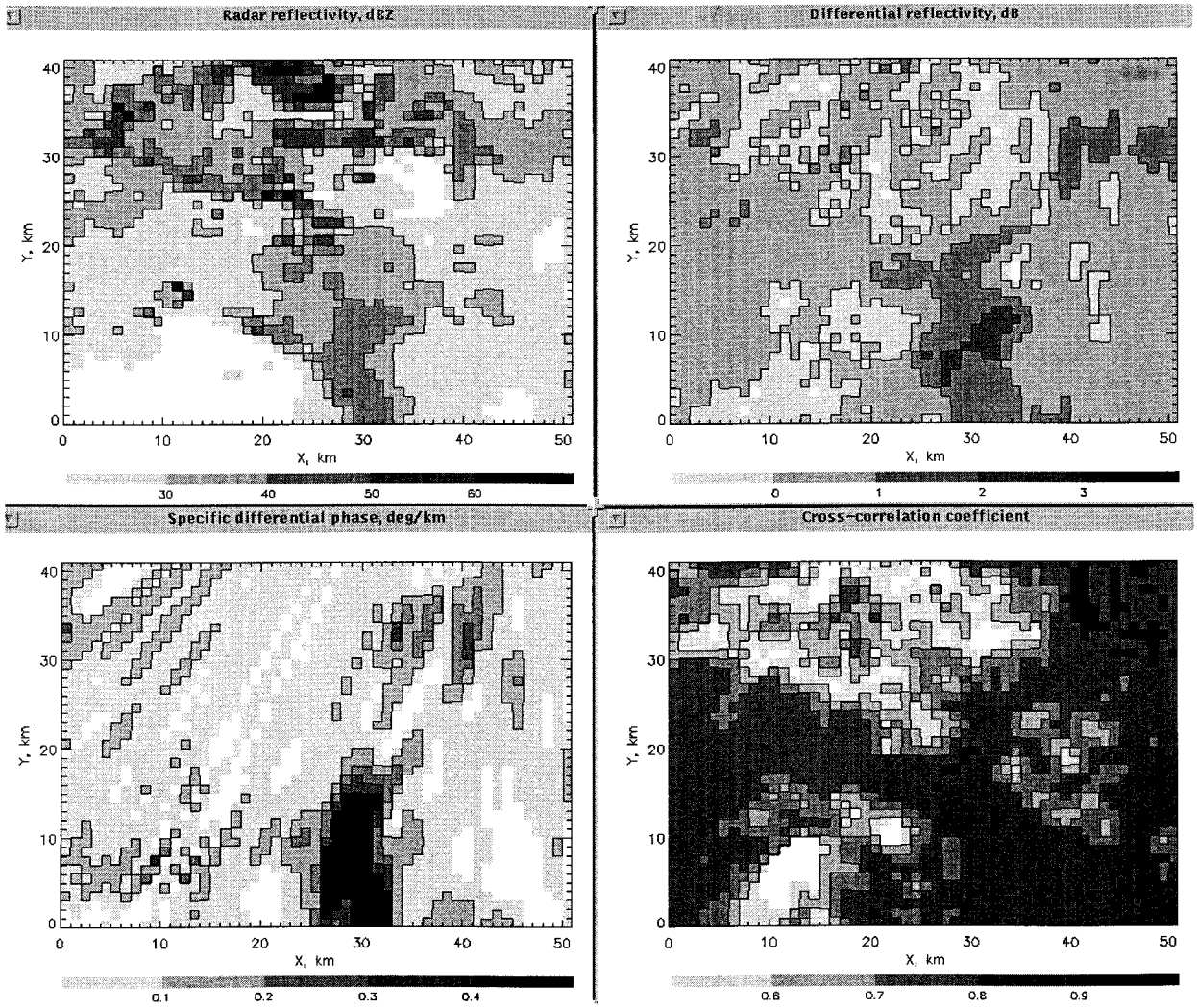

FIG. 5. Composite plot of (a) Z, (b) Z_{DR}, (c) K_{DP}, and (d) ρ_{hv} in the test area for the storm of 30 June 1994. The time is 0547 UTC. Contours of Z are 10 dB apart, starting at 30 dBZ. The Z_{DR} contours are in steps of 1 dB, starting at 0 dB. The K_{DP} contours are drawn in steps of 0.1° km^{-1} beginning at 0.1° km^{-1}. Here ρ_{hv} is contoured in 0.1 increments starting at 0.6.

mean rain rate $\langle R \rangle = 5.2$ mm h^{-1} as a gauge total areal accumulation divided by the product of the watershed area and the rain duration time (1 h in this case). The Marshall–Palmer algorithm overestimates (6.6 mm h^{-1}) the mean rain rate due to contribution from AP, whereas the polarimetric estimates $\langle R \rangle = 4.7$ mm h^{-1} and $\langle R \rangle = 4.8$ mm h^{-1} (for the smaller and larger averaging windows) are closer to the rain gauge's mean. Note that in this rain event the effect of the averaging interval for the K_{DP} estimation is negligible.

Gauges have higher rain accumulation in the northeast corner of the image compared to both conventional and polarimetric radar estimates that are consistent with each other. The discrepancy is likely due to wrong readings of gauge accumulation from strip charts. Gauges in the test area are not automated, and time reference errors of about 10–15 min are quite possible. This might lead to the errors in 1-h accumulations for some gauges, especially in convective events in which temporal changes of rain rates are much higher than in stratiform rain. There is a possibility that compensating errors elsewhere in the grid minimize the mean error for the whole watershed area. Generally, time reference errors do not significantly affect mean rain rate in predominantly stratiform precipitation if $\langle R \rangle$ is low, as in this particular case.

In the case of 30 June 1994, the polarimetric algorithm successfully eliminates AP contamination because AP appears in isolated regions immersed in the rather uniform precipitation background, where uncorrupted estimates of specific differential phase and rain rate are available. Therefore, the relatively simple procedure of bridging the gaps is successful. Good performance of the K_{DP}-based algorithm is also expected if signal powers from precipitation and ground clutter are comparable, so that the cross-correlation coefficient of the mix-

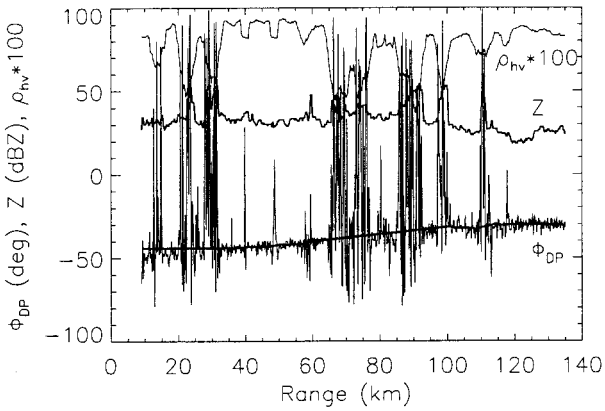

FIG. 6. An example of radial dependencies of Φ_{DP}, Z, and ρ_{hv} in the precipitation region contaminated with AP. The date is 30 June 1994 and the time is 0537 UTC. El = 0.5° and Az = 228.1°. Smoothed Φ_{DP} data have been obtained after averaging over 48 successive range gates (8.6 km).

ture is still above 0.7 and SD(Φ_{DP}) is below the threshold of 12°. Under these circumstances an unbiased estimate of K_{DP} is possible, although with larger statistical error. This is probably the case for the storms of 7 October 1996 and 18 July 1997 examined in the previous section. The ρ_{hv} was between 0.75 and 0.85 in the region with reflectivities of 50 or more dBZ, as shown in Fig. 1.

The polarimetric method for rainfall estimation has only limited application if ground clutter completely dominates precipitation echo in most of the coverage area. Such was the case of 8 July 1996 (Figs. 8 and 9). It can be seen from Fig. 8 that only a small portion of the radar echo is not affected by the AP ground clutter at the elevation of 0.5° ($\rho_{hv} > 0.7$). Moreover, examination of reflectivity pattern at the elevation angle of 1.5° indicates that the noncontaminated echo region constitutes a very small part of the rainy area; that is, the echo area with $\rho_{hv} > 0.7$ in Fig. 8b is much smaller than the precipitation areas in Figs. 9a or 9b, both of which are almost unaffected by AP. Thus, Doppler clutter filtering (Weber et al. 1993) and height continuity need to be combined with polarimetry to help mitigate the effects of AP in a variety of practical situations.

4. Conclusions

We have applied radar polarimetry to identify the areas of weather echoes contaminated by AP and to estimate rainfall in the presence of ground clutter returns caused by anomalous propagation. Data collected with the NSSL's polarimetric radar (wavelength 10 cm) were used for this analysis. Ground truth rainfall data have been obtained from the Oklahoma Mesonet and the special test area containing 42 densely spaced gauges in the Little Washita River Basin, which is situated between 45 and 80 km from the radar.

Simple analysis of the cross-correlation coefficient ρ_{hv} between horizontally and vertically polarized radar returns identifies the regions of AP. The radar echo is contaminated with AP-induced ground clutter if the corresponding ρ_{hv} is below a certain threshold, ρ_t, and well above zero. The threshold $\rho_t = 0.7$ is a reasonable selection at least for the Cimarron polarimetric radar data.

A standard deviation of differential phase SD(Φ_{DP}) is closely related to the magnitude of the cross-correlation coefficient and also can be used to localize the areas of AP. The SD(Φ_{DP}) threshold of 10°–12° is a good choice for the Cimarron radar data.

If relative contributions of precipitation and AP-induced ground clutter to radar signal are of the same order of magnitude, then the specific differential phase K_{DP} can still be effective for rainfall measurement. This is because ground clutter does not bias the total differential phase Φ_{DP} but only increases its fluctuations; hence, K_{DP} can yield a rain estimate free of clutter contamination.

If ground clutter totally dominates precipitation echo, then pointwise polarimetric estimates of rain rate are impossible in the contaminated area. Nevertheless, if AP appears in isolated regions immersed in rather uniform precipitation background, then the averaged values of K_{DP} (and rain rate) can be restored in the heavily contaminated areas provided that uncorrupted measurements of K_{DP} outside the AP areas are available. This technique was successfully demonstrated in the AP case of 30 June 1994, whereby hourly rain accumulation over a watershed-size area computed using this polarimetric technique compared much better with rain gauges than with that obtained from the radar reflectivity factor. It is premature to extrapolate our results because only this one case had ground truth data from the gauge micronetwork. Additional cases with verifiable rain accumulations in the presence of AP are needed to confirm this preliminary study.

Standard Doppler filtering technique for eliminating AP echoes can be used in addition, or as an alternative, to the suggested polarimetric algorithm, especially if ground clutter heavily dominates the precipitation echo in most of the radar coverage area. Intuition suggests that the combined Doppler and polarimetric method for dealing with the clutter should offer greatest benefits. Nonetheless, it is not known how much improvement this would be over the optimum Doppler method because such a scheme has not yet been established. An obvious extension of the classic filtering would be to extrapolate rainfall in the clutter region—for example, by judiciously comparing the filtered and nonfiltered data. This certainly requires more study.

Acknowledgments. The authors appreciate the assistance of H. Johnson, from the Oklahoma Climatological Survey, and Dr. R. Lopez, from NSSL, who provided the Oklahoma Mesonet rain gauge data. T. Schuur's review improved the style. G. Heathman of the U.S. Agricultural Research Station in Chikasha, Oklahoma, pro-

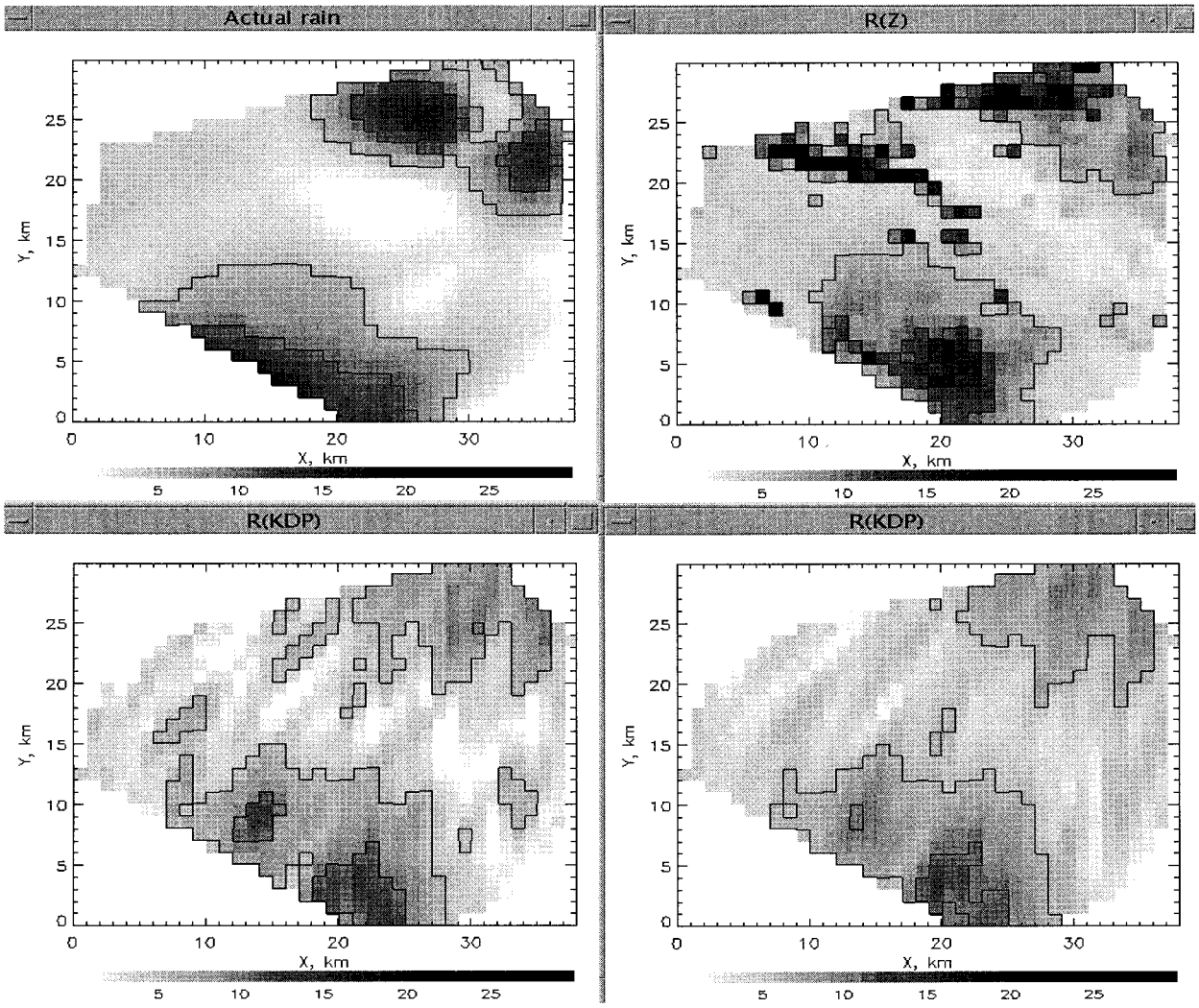

FIG. 7. A 1-h rain depth map in the test area obtained (a) from the gauges, (b) from the polarimetric radar using $R(Z)$, (c) using $R(K_{DP})$ with a smaller averaging window, and (d) using $R(K_{DP})$ with a larger averaging window. Contours of rain accumulation are in 5 mm h^{-1} increments, starting from 5 mm h^{-1}.

vided the charts of rainfall accumulation in the ARS test area. The National Weather Service Office of hydrology provided partial support for this work.

APPENDIX

Standard Deviation of the Differential Phase Estimate

Standard deviation of the differential phase estimate (Φ_{DP}) was first examined by Sachidananda and Zrnic (1986) as a function of the cross-correlation coefficient, the Doppler spectrum width, and the number of radar samples for alternate switching between two orthogonal polarizations. Here, we derive a relatively simple formula for the SD(Φ_{DP}) as a function of the cross-correlation coefficient ρ_{hv} but for the simultaneous transmission and reception of orthogonally polarized radar returns. The simultaneous transmission–reception scheme is considered for prototyping on a research WSR-88D radar at NSSL. We then compare the results for simultaneous transmission with the ones for alternate transmissions.

Using M synchronous H, V sample pairs, we define an estimator of differential phase Φ_{DP} as

$$\hat{\Phi}_{DP} = \arg(\hat{U}), \tag{A1}$$

where

$$\hat{U} = \frac{1}{M}\sum_{i=1}^{M} \langle H_i V_i^* \rangle. \tag{A2}$$

The asterisk represents the complex conjugate, and the hat indicates the estimates. Following Sachidananda and Zrnic (1986), the variance of the Φ_{DP} estimate can be

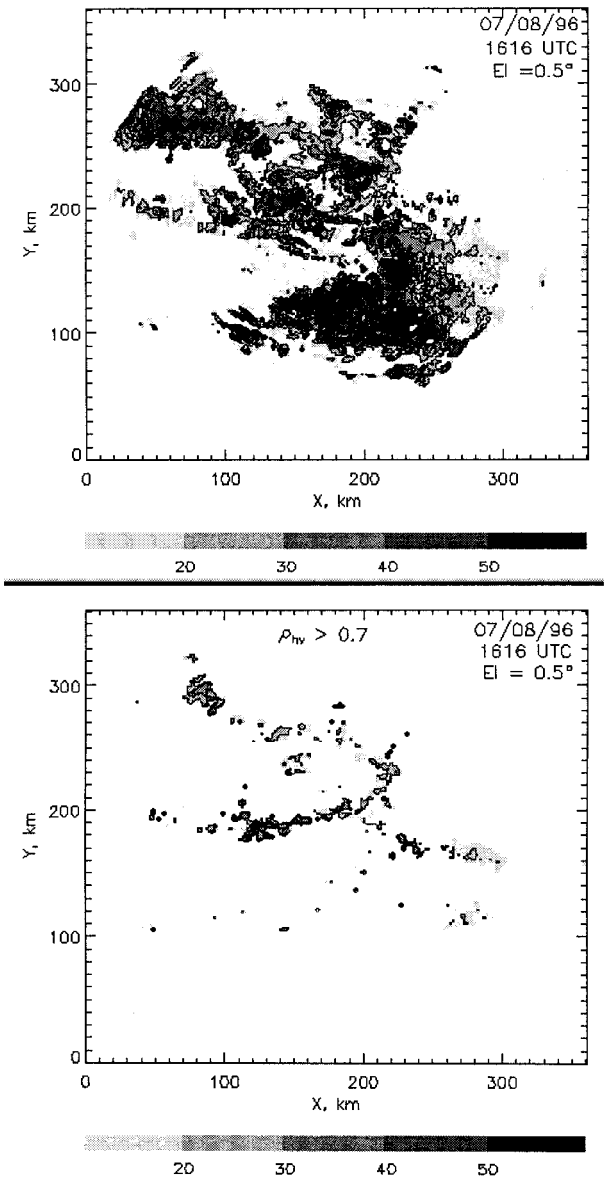

FIG. 8. The field of Z at an elevation of 0.5° for the 8 July 1996 storm. In the lower plot, data with $\rho_{hv} > 0.7$ are shown. The time is 1616 UTC. Contours of Z are 10 dB apart, starting at 20 dBZ.

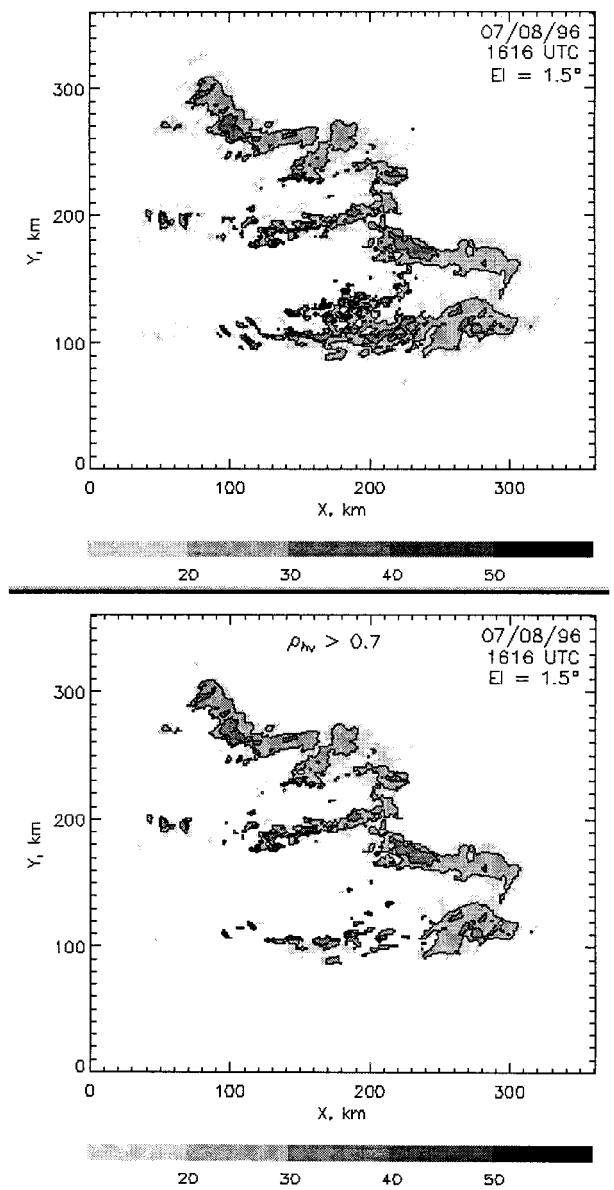

FIG. 9. Same as in Fig. 8 but the elevation angle is 1.5°.

expressed in terms of $\hat{U}$ and $\overline{U}$ as ($\overline{U}$ is the mean value of $\hat{U}$)

$$\mathrm{var}(\hat{\Phi}_{\mathrm{DP}}) = \frac{1}{2}\mathrm{Re}\left[\left\langle\left|\frac{\hat{U}}{\overline{U}}\right|^2\right\rangle - \left\langle\left(\frac{\hat{U}}{\overline{U}}\right)^2\right\rangle\right]. \quad \text{(A3)}$$

The expected values of $|\hat{U}|^2$ and $(\hat{U})^2$ are

$$\langle|\hat{U}|^2\rangle = \frac{1}{M^2}\left\langle\sum_{i=1}^{M}\sum_{j=1}^{M}\mathrm{H}_i\mathrm{V}_i^*\mathrm{H}_j^*\mathrm{V}_j\right\rangle \quad \text{(A4)}$$

and

$$\langle(\hat{U})^2\rangle = \frac{1}{M^2}\left\langle\sum_{i=1}^{M}\sum_{j=1}^{M}\mathrm{H}_i\mathrm{V}_i^*\mathrm{H}_j\mathrm{V}_j^*\right\rangle. \quad \text{(A5)}$$

To proceed further we need the identities

$$\langle\mathrm{H}_i\mathrm{V}_i^*\mathrm{H}_j^*\mathrm{V}_j\rangle = \langle\mathrm{H}_i\mathrm{V}_i^*\rangle\langle\mathrm{H}_j^*\mathrm{V}_j\rangle + \langle\mathrm{H}_i\mathrm{H}_j^*\rangle\langle\mathrm{V}_i^*\mathrm{V}_j\rangle \quad \text{(A6)}$$

and

$$\langle\mathrm{H}_i\mathrm{V}_i^*\mathrm{H}_j\mathrm{V}_j^*\rangle = \langle\mathrm{H}_i\mathrm{V}_i^*\rangle\langle\mathrm{H}_j\mathrm{V}_j^*\rangle + \langle\mathrm{H}_i\mathrm{V}_j^*\rangle\langle\mathrm{H}_j\mathrm{V}_i^*\rangle, \quad \text{(A7)}$$

$$\langle\mathrm{H}_i\mathrm{V}_i^*\rangle = \sqrt{P_{\mathrm{h}}P_{\mathrm{v}}}\,\rho_{\mathrm{hv}}, \quad \text{(A8)}$$

$$\langle\mathrm{H}_i^*\mathrm{V}_i\rangle = \sqrt{P_{\mathrm{h}}P_{\mathrm{v}}}\,\rho_{\mathrm{hv}}^*, \quad \text{(A9)}$$

and express the second moments through auto- and cross-correlation coefficients

$$\langle \mathrm{H}_i \mathrm{H}_j^* \rangle = P_\mathrm{h} r(m), \tag{A10}$$

$$\langle \mathrm{V}_i^* \mathrm{V}_j \rangle = P_\mathrm{v} r^*(m), \tag{A11}$$

$$\langle \mathrm{H}_i \mathrm{V}_j^* \rangle = \sqrt{P_\mathrm{h} P_\mathrm{v}}\, r_\mathrm{hv}(m), \tag{A12}$$

and

$$\langle \mathrm{H}_j \mathrm{V}_i^* \rangle = \sqrt{P_\mathrm{h} P_\mathrm{v}}\, r_\mathrm{hv}(-m), \tag{A13}$$

where $m = i - j$, P_h and P_v are the powers of horizontally and vertically polarized components of the signal, ρ_hv is a cross-correlation coefficient, $r_\mathrm{hv}(m) = \rho_\mathrm{hv} r(m)$, and

$$r(m) = \exp(j2k\upsilon Tm) \exp(-8\pi^2\sigma_\upsilon^2 T^2 m^2/\lambda^2) \tag{A14}$$

is the autocorrelation coefficient. In (A14), $k = 2\pi/\lambda$, υ is mean Doppler velocity, T is pulse repetition time, σ_υ is Doppler velocity spectrum width, and λ is radar wavelength. For the sake of simplicity, receiver noise was ignored in the formulas (A8)–(A14). After substituting (A8)–(A13) into (A4) and (A5) and keeping in mind that

$$\overline{U} = \sqrt{P_\mathrm{h} P_\mathrm{v}}\, \rho_\mathrm{hv}, \tag{A15}$$

we finally arrive at the following equations:

$$\left\langle \left| \frac{\hat{U}}{\overline{U}} \right|^2 \right\rangle = 1 + \frac{1}{M^2} \sum_{m=-(M-1)}^{M-1} (M - |m|) \frac{|r(m)|^2}{|\rho_\mathrm{hv}|^2}, \tag{A16}$$

and

$$\left\langle \left(\frac{\hat{U}}{\overline{U}} \right)^2 \right\rangle = 1 + \frac{1}{M^2} \sum_{m=-(M-1)}^{M-1} (M - |m|) |r(m)|^2. \tag{A17}$$

Combining (A16) and (A17) in (A3), we obtain

$$\begin{aligned} \mathrm{SD}(\Phi_\mathrm{DP}) &= [\mathrm{var}(\Phi_\mathrm{DP})]^{1/2} \frac{180}{\pi} \\ &= \frac{180}{\pi} \frac{1}{(2M_I)^{1/2}} (|\rho_\mathrm{hv}|^{-2} - 1)^{1/2}. \end{aligned} \tag{A18}$$

In (A18), the $\mathrm{SD}(\Phi_\mathrm{DP})$ is expressed in degrees; $M_I = M/\mu$ is a number of equivalent independent samples (Doviak and Zrnic 1993), where

$$\mu = \sum_{m=-(M-1)}^{M-1} \left(1 - \frac{|m|}{M} \right) |r(m)|^2. \tag{A19}$$

For typical values of the radar wavelength $\lambda = 10$ cm and PRF = 1000 Hz, the parameter μ is equal to 3.9, if $\sigma_\upsilon = 4$ m s^{-1} and $\mu = 15.5$ if $\sigma_\upsilon = 1$ m s^{-1}. The combination of $M = 60$ and $\rho_\mathrm{hv} = 0.995$ yields $\mathrm{SD}(\Phi_\mathrm{DP}) = 0.72°$ and $\mathrm{SD}(\Phi_\mathrm{DP}) = 1.45°$ for $\sigma_\upsilon = 4$ and 1 m s^{-1}.

Following Sachidananda and Zrnic (1986), the perturbation analysis produces a formula similar to (A19) for the variance of Φ_DP:

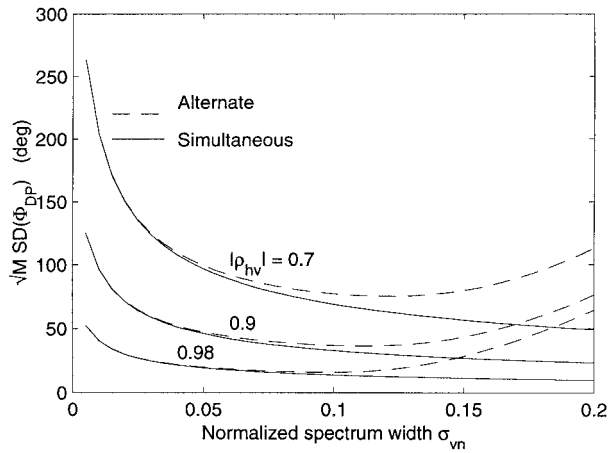

FIG. A1. Here $\sqrt{M}\,\mathrm{SD}(\Phi_\mathrm{DP})$ is a function of the normalized spectrum width $\sigma_\mathrm{vn} = 2\sigma_\upsilon T/\lambda$ for alternate and simultaneous transmission–reception; M is the total number of transmitted pulses.

$$\begin{aligned} \mathrm{var}(\Phi_\mathrm{DP}) = &\frac{1 - |\rho_\mathrm{hv}|^2 r^2(1)}{4L^2|\rho_\mathrm{hv}|^2} \sum_{m=L-1}^{L-1} (L - |m|) r^2(2m) \\ &- \frac{|\rho_\mathrm{hv}|^2 - r^2(1)}{4L^2|\rho_\mathrm{hv}|^2} \sum_{m=L-1}^{L-1} (L - |m|) r^2(2m+1), \end{aligned} \tag{A20}$$

where L is the number of H, V pairs and equals $M/2$. Note that for the same dwell time (MT_s), there are twice as many pairs of H, V echoes in simultaneous transmission as there are in alternate transmission. The plot (Fig. A1) of the standard deviations corresponding to the two formulas illustrates the difference between the two. For narrow spectra (compared to the unambiguous interval), the two schemes are equivalent; the samples are highly correlated and the errors primarily depend on the dwell time. At larger spectrum widths, the alternate scheme is clearly inferior: a sharp increase in the error is observed at a normalized spectral width of about 0.12. This is where the decorrelation of samples degrades the estimates, and such a condition is clearly absent for simultaneous transmission, whereby the orthogonal simultaneous echoes are tightly correlated. At a radar wavelength of 10 cm and typical T of 1 m s^{-1}, $\sigma_\mathrm{vn} < 0.12$ corresponds to $\sigma_\upsilon < 6$ m s^{-1}. Therefore, alternate and simultaneous transmission–reception schemes are almost equivalent, provided that the total dwell times are the same. At higher microwave frequencies (5- and 3-cm wavelengths), simultaneous transmission gives a lower $\mathrm{SD}(\Phi_\mathrm{DP})$ for wide Doppler spectra. Note also that $\mathrm{SD}(\Phi_\mathrm{DP})$ is always lower for longer PRT in the case of simultaneous transmission.

The standard deviation of the Φ_DP estimate exhibits strong dependence on the cross-correlation coefficient ρ_hv. In accordance with (A18), changing ρ_hv from 0.95 to 0.7 leads to more than a threefold increase in the $\mathrm{SD}(\Phi_\mathrm{DP})$.

REFERENCES

Bean, B. R., and E. J. Dutton, 1966: *Radio Meteorology.* Dover Publications, 435 pp.

Doviak, R. J., and D. S. Zrnic, 1993: *Doppler Radar and Weather Observations.* Academic Press, 562 pp.

Moszkowicz, S., G. Ciach, and W. Krajewski, 1994: Statistical detection of anomalous propagation in radar reflectivity patterns. *J. Atmos. Oceanic Technol.,* **11,** 1026–1034.

Pratte, F., R. J. Keeler, R. Gagnon, and D. Sirmans, 1995: Clutter processing during anomalous propagation conditions. Preprints, *27th Conf. on Radar Meteorology,* Vail, CO, Amer. Meteor. Soc., 139–141.

Ryzhkov, A. V., and D. S. Zrnic, 1996: Assessment of rainfall measurement that uses specific differential phase. *J. Appl. Meteor.,* **35,** 2080–2090.

——, V. B. Zhuravlyov, and N. A. Rybakova, 1994: Preliminary results of X-band polarization studies of clouds and precipitation. *J. Atmos. Oceanic Technol.,* **11,** 132–139.

Sachidananda, M., and D. S. Zrnic, 1986: Differential propagation phase shift and rainfall rate estimation. *Radio Sci.,* **21,** 235–247.

——, and ——, 1987: Rain rate estimates from differential polarization measurements. *J. Atmos. Oceanic Technol.,* **4,** 588–598.

Weber, M., M. Stroke, and J. Cullen, 1993: Anomalous propagation associated with thunderstorms outflow. Preprints, *26th Int. Conf. on Radar Meteorology,* Norman, OK, Amer. Meteor. Soc., 238–240.

Zahrai, A., and D. S. Zrnic, 1993: The 10-cm-wavelength polarimetric weather radar at NOAA's National Severe Storms Laboratory. *J. Atmos. Oceanic Technol.,* **10,** 649–662.

Zrnic, D. S., and A. V. Ryzhkov, 1996: Advantages of rain measurements using specific differential phase. *J. Atmos. Oceanic Technol.,* **13,** 454–464.